# Ultrasound texture based assessment of fetal pulmonary risk

K. N. Bhanu Prakash and A. G. Ramakrishnan
Biomedical Lab., Dept. of Electrical Engg, Indian Institute of Science,
Bangalore -560 012. Karnataka, INDIA.

**Abstract**–This pilot study was carried out to find the feasibility of analyzing the maturity of the fetal lung using ultrasound images. Data were collected from 350 pregnant women at intervals of 2 weeks from the gestation age of 24 to 38 weeks. Various textural features were computed from regions of interest of $64 \times 64$ pixels each from the fetal lung and liver images. The ratios of fetal lung to liver feature values were investigated as possible indices for classifying the images into those from mature (reduced pulmonary risk) and immature (possible pulmonary risk) lung. The features used are fractal dimension, lacunarity and features derived from the histogram of the images. Classifiers such as nearest-neighbour (NN), k-NN, modified k-NN, multilayer perceptron, radial basis function network and support vector machines were used. A classification accuracy of 73 to 96% was obtained for the test set.

Index terms–Fetal lung; Lung maturity; Sonogram; Texture; Fractal dimension; Classification.

## I. Fetal lung maturity analysis

Prenatal diagnosis (PD) is essential to avoid an untoward outcome for the fetus or the mother or both. The assessment of fetal lung maturity is of great value in perinatal management. A variety of techniques are available for PD. However, all the current techniques for PD are invasive, involving at least a sample of maternal blood. In amniocentesis, the study of Lecithin - Sphingomyelin (L/S) ratio is the most useful. However, being invasive, it carries risks, and on occasion, may be contraindicated. Ultrasonography is a non-invasive procedure, which can currently be used to determine fetal size, gestation age (GA), and the condition of placenta.

There has been extensive debate for and against the use of sonographic features for analyzing fetal lung maturity. Thieme et al [1] studied the lung development in the lamb through sonographic patterns. Garrett et al. [2] stated that reflectivity of human fetal lung is equal to or less than that of liver throughout most of pregnancy but that relationship reverses in late gestation. Cayea et al. [3] argued that there is no statistically significant correlation between the sonographic features and the biochemical fetal lung maturity indices, namely L/S ratio and phosphatidylglycerol values. Benson et al. [4] employed RF signals for characterizing fetal lung and liver tissues. They observed a spectral shift in the reflected signals from a high to a low frequency range, when the lung makes a transition from immature to mature state. Feingold et al. [5] used densitometer measurements to establish a correlation between lung-liver echogenicity and L/S ratio. Podobnik et al. [6] developed a relation between the coefficient of variation of lung -liver echogenicity and L/S ratio. Petrucha et al. [7] measured biparietal diameter (BPD) and placental grading (PG) from ultrasound. They concluded that BPD together with PG is at least as sensitive as the L/S ratio in predicting the pulmonary maturity. Sohn et al. [8] carried out frequency analysis of both fetal lung and liver and the ratio between the mean and the range of the frequencies received was used as an index of maturity analysis.

Some of the earlier studies have used echogenicities of the lung and liver as possible indices of pulmonary maturity [5], [2], [8]. Many researchers have used textural measures to study and analyze the liver texture in differential diagnosis of liver [9], [10]. Ultrasound cannot measure any of the biochemical parameters of fetal lung maturity, nor can it provide direct histologic information about fetal lung development. However, it is reasonable to assume that both morphological and biochemical changes alter the diffuse scattering and other propagation properties of fetal lung. This may change the textural appearance of sonogram. Since echogenicity is sensitive to machine settings and textural features have been used in the literature for the differential diagnosis of liver, we attempted to classify lung images as belonging to mature or immature class using textural features. The motivation was to find the possible changes in the sonogram texture during the transition from a high pulmonary risk group to a low pulmonary risk group.

## II. Data Collection

Ultrasound examinations were performed both at Mediscan Systems, Chennai, India and at the University Hospital in Kuala Lumpur, Malaysia. Data were collected in both places using the real time ATL Apogee 800 plus scanner with a 3.5 MHz curvilinear, broad bandwidth transducer probe with the dynamic range set at 55 dB. Imaging was performed in a similar way at both locations. The overall gain was set at an optimal value to get uniform visibility. Longitudinal and transverse sections of the fetal thorax and upper abdomen were imaged. The fetal lung and liver were identified in the thoracic and upper abdominal sections, respectively. Obvious vascular structures in the liver were avoided. An uniform echo texture was obtained by optimizing the machine settings. The post-processing curves were unchanged. The focal zone was adjusted to keep the area of interest always in focus. Data were collected from 350 subjects belonging to Indian, Chinese and Malay races at gestation ages from 24 to 38 weeks, at intervals of 2 weeks. Since most deliveries after 34 weeks can be effectively handled with medical support, and since there is little incidence of pulmonary risk after 38 weeks, data was collected only up to 38 weeks. Further, in most Asian races, pregnancy ends around 38 weeks. In this paper, we refer to the group with pulmonary risk as immature and the one with reduced risk as mature. Since it is known clinically that many babies at 34 weeks of gestation do not have pulmonary risk, we have considered subjects above 35 weeks as belonging to the mature class. The subjects were followed up throughout the pregnancy and also after delivery. Only the data corresponding to normal pregnancies, also leading to babies with normal pulmonary functions, were included in our analysis.

A cross-sectional study of normal fetuses have shown that the overall size of a fetus at each GA falls within a range of $5^{th}$ to $95^{th}$ centile. Hence, in our study, since normal subjects are chosen, large variations in depth were not encountered. The lung and the liver areas taken for analysis were contiguous and at the same depth for each fetus. The appropriate section of each image was frozen and then transferred to videotape. The images were then digitized using the Creative video grabber card with 8-bit resolution. The size of the digitized image was $320 \times 240$ pixels with a resolution of 29 pixels per cm. The histogram of the images was stretched to occupy the entire range of gray values. Regions of interest (ROI) of $64 \times 64$ pixels each from the liver and the lung regions were used for extracting textural features. Figure 1 shows two fetal echogram samples, with the ROI's selected from the liver and lung regions. Figure 2 displays the selected regions of interest from both the lung and liver regions from one sample image each belonging to the different GA's. The total data acquired consisted of 750 images of immature class and 250 images of mature class. The lung to liver ratio of various feature values were studied as possible indices of maturity.

## III. Feature Extraction

The textural features extracted are described below.

*Spatial gray level dependence matrices (SGLDM):* These are based on the second order joint conditional probability density functions, $f_{\phi,d}(a,b)$. Here $f_{\phi,d}(a,b)$ is the probability that a pair of pixels separated by a distance $d$ at an angle $\phi$ have gray levels $a$ and $b$. Haralick [11] proposed 14 texture measures that can be extracted from the estimated probability density functions, $P_{\phi,d}(a,b)$. In our study, only the following five texture features are computed.

$$Energy = \sum_a \sum_b \left[P_{\phi,d}(a,b)\right]^2 \tag{1}$$

$$Entropy = -\sum_a \sum_b P_{\phi,d}(a,b) log\ P_{\phi,d}(a,b) \tag{2}$$

$$Inertia = \sum_a \sum_b (a-b)^2 P_{\phi,d}(a,b) \tag{3}$$

$$L = \sum_a \sum_b \frac{1}{1+(a-b)^2} P_{\phi,d}(a,b) \tag{4}$$

$$C = \frac{1}{\sigma_x \sigma_y} \sum_a \sum_b (a-\mu_x)(b-\mu_y) P_{\phi,d}(a,b) \tag{5}$$

$\mu_x = \sum_a a \sum_b P_{\phi,d}(a,b)$
$\sigma_x^2 = \sum_a (a-\mu_x)^2 \sum_b P_{\phi,d}(a,b)$
where the two summations are carried over all the values of $a \in (0, N_G - 1)$ and $b \in (0, N_G - 1)$, respectively, $N_G$ is the number of gray levels in the image and C, L are the correlation and the local homogeneity, respectively. Similarly, $\mu_y$ and $\sigma_y$ are computed. Each measure is evaluated for $d = 1$ and $\phi = 0^o, 45^o, 90^o$ and $135^o$.

*Gray level difference matrix (GLDM):* Let $I(x,y)$ be the image intensity function. For any given displacement $\delta = (\Delta x, \Delta y)$, let $I_\delta(x,y) = |I(x,y) - I(x+\Delta x, y+\Delta y)|$, and $f'(i|\delta)$ be the probability density of $I_\delta(x,y)$. If there are $m$ gray levels, this has the form of an m-dimensional vector whose $i^{th}$ component is the probability that $I_\delta(x,y)$ will have value $i$. $f'(i|\delta)$ is obtained as the number of times $I_\delta(x,y)$ has a value of $i$ for a given $\delta$, i.e.,

$$f'(i|\delta) = P(I_\delta(x,y) = i)$$

Four forms of the vector $\delta$ were considered: $(0,d)$, $(-d,d)$, $(d,0)$ and $(-d,-d)$ where $d$ is the interpixel distance. From each of the density functions, the following five texture features were extracted:

$$Conrast : CON = \sum_i i^2 f'(i|\delta) \tag{6}$$

$$MEAN : \sum_i i f'(i|\delta) \tag{7}$$

$$Entropy : ENT = \sum_i f'(i|\delta) log(f'(i|\delta) \tag{8}$$

$$IDM = \sum_i f'(i|\delta)/(i^2+1) \tag{9}$$

$$ASM = \sum_i [f'(i|\delta)]^2 \tag{10}$$

where IDM and ASM are the inverse difference moment and angular second moment, respectively and the subscript $i \in (0, N_G - 1)$ in all the cases.

*Laws' textural measures:* Laws' textural energy measures [12] are derived from three vectors, each of length three: $L3 = \{1,2,1\}$, $E3 = \{-1,0,1\}$ and $S3 = \{-1,2,-1\}$. These respectively represent the operations of local averaging, edge detection and spot detection. If these vectors are convolved with themselves or with one another, we obtain among others the following three vectors, each of length five: $L5 = \{1,4,6,4,1\}$, $S5 = \{-1,0,-2,0,-1\}$ and $E5 = \{$-1,$-2,0,2,1,\}$ which perform local averaging, spot and edge detection, respectively. The masks used in our analysis are $L5^T E5$ and $L5^T\ S5$. The masks were convolved with the image and the entropy of the resulting image was calculated.

*Fractal dimension and Lacunarity:* The fractal dimension (FD) is computed based on the concepts of multiresolution image analysis and fractional Brownian motion model (fBMM). The intensity surface of an ultrasonic image can be viewed as the end result of random walks, and fBMM [13] can be used for its analysis. FD and lacunarity are the important features that characterize the roughness and granularity of the fractal surface. Given an $MXM$ image $I$, the intensity difference vector (IDV) is defined as $IDV = [id(1), id(2), ...id(s)]$ where s is the maximum possible scale and $id(k)$ is the average of the absolute intensity difference of all pixel pairs with horizontal or vertical distance k. We compute $id(k)$ as

$$id(k) = \frac{1}{2M(M-k-1)}$$
$$\sum_{i=0}^{M-1} \sum_{j=0}^{M-k-1} | I(i,j) - I(i,j+k) |$$
$$+ \sum_{i=0}^{M-k-1} \sum_{j=0}^{M-1} | I(i,j) - I(i+k,j) | \qquad (11)$$

and $FD = 3 - H$, where $H$ is the Hurst parameter. $H$ is estimated as the slope of the curve of $id(k)$ versus $k$ in log-log scale, using least-squares linear regression. Given a fractal set $A$, let $P(m)$ be the probability that there are m points within a box of size $L$, centered about an arbitrary point of $A$. We have, $\sum_{m=1}^{N} P(m) = 1$, where $N$ is the number of possible points within the box. The lacunarity is defined as

$$\wedge = (M_2 - M^2)/M^2 \qquad (12)$$

where $M = \sum_{m=1}^{N} mP(m)$ and $M_2 = \sum_{m=1}^{N} m^2 P(m)$

*Histogram based features:* The histogram based features calculated were mean, variance, coefficient of variation (CV), skewness, kurtosis and second moment (SM).

Out of the 64 features extracted, the features of GLDM and SGLDM had similar variations. Since computation of SGLDM features is both time and memory consuming, we discarded those features. The features which were retained are FD, intercept, lacunarity, CON, ENT, IDM, ASM, MEAN from GLDM, entropy of Law's textural measures, Mean, Variance, CV, skewness, SM and kurtosis from histogram of the images. Based on Pearson's correlation test, the following 6 features that exhibited good correlation with GA are selected: (i) FD, (ii) lacunarity from fractal measures, (iii) mean, (iv) variance, (v) CV, and (vi) SM calculated from the histogram. The ratios of these features were used as input to the classifiers. It was observed that data sets from both the hospitals exhibited similar behavior.

## IV. Training and test data sets

The collected data was grouped into two classes: Samples from 24 to 34 weeks of gestation were considered to belong to the immature class (possibility of pulmonary risk) and those from 36 to 38 weeks, as mature (reduced risk), as pulmonary risk is very rare after 35 weeks of gestation. Three different types of training and test sets were formed from the samples. The first set had 800 training and 200 test samples. Of the training data, 600 belonged to the immature class and 200, to mature class. The test set contained 150 samples of immature class and 50 of mature class. In the second training set, 400 samples were from 24 to 30 weeks of gestation, and 200, from 36 to 38 weeks of gestation. In the test set, 200 samples belonged to 32 to 34 weeks of gestation and 50 belonged to 36 to 38 weeks of gestation. The third set contained 400 training samples, with equal number from immature and mature classes. To form the test set of 100 samples, an equal number of immature and mature samples were randomly picked from the total data set. In our training, we have considered immature lung classified as immature as true positive (TP).

## V. Classifiers used for the study

The ultrasonic images were classified into mature and immature classes using the following classifiers.

*Nearest-neighbour (NN) classifier:* This assigns an unknown sample a class same as that of the sample in the training set nearest to it in the feature space by Euclidean distance.

*k-nearest neigbour (k-NN) classifier:* There is a possibility of NN classifer yielding an erroneous decision if the obtained single neighbor is an out-lier of some other class. To avoid this and improve the robustness of the approach, the k-NN classifier works with k patterns in the neighborhood of the test pattern. In our study, the value of $k$ was chosen to be 7 after testing with a number of values of k.

*Modified k-nearest neighbor (mk-NN) classifier:* In the $k$-NN classifier, though a search in the k-neighborhood drives classification, the distance of a template from the test character does not play any role. In an effort to bring about a weighted representation, the m$k$-NN classifier associates a distance-based weight with each prototype member in the $k$-neighborhood. This weighted representation schedule then drives the classification process. The weight is calculated as follows:

Let $\mathcal{S} = \{s_1, s_2, \ldots, s_k\}$ be the set of reference patterns in the $k$ neighborhood of the test pattern in the feature space, sorted in the increasing order of their distances from the test pattern. Let $\mathcal{X} = \{x_1, x_2, \ldots, x_k\}$ be the respective distances from the test pattern, where $x_1$ is the minimum and $x_k$ is the maximum distance. Let $\mathcal{W} = \{w_1, w_2, \ldots, w_k\}$ be a weight set with $w_i$ as the weight assigned to pattern $s_i$ based on its distance from the test feature vector, given as:

$$w_i = (x_k - x_i)/(x_k - x_1) \qquad (13)$$

By testing with different values of $k$, we found that $k = 7$ gave a classification accuracy better than any other value.

*Multilayer perceptron (MLP):* The MLP is a feedforward network, capable of generating nonlinear boundaries. In our study, a two layer network was chosen with 6 input nodes, one hidden layer with 3 nodes and 2 output nodes. The hidden layer had sigmoid activation function, whereas the output nodes had linear activation function.

*Radial basis function network (RBF):* The RBF network [14] performs interpolation in a multidimensional space.

The RBF network has a high dimensional hidden layer with Gaussian kernels. In the current study, a network with six input nodes, fifteen hidden nodes and two output nodes was used. The centres of the Gaussian kernels were estimated through k-means algorithm.

*Support vector machines (SVM):* In SVM [15], the optimal hyper-plane decides the separation between individual classes of patterns. The optimality is in the following sense: the average distance between the hyper-plane and the closest training points on both sides is maximal. This aids in maximization of the correct classification rate. Whereas data with linear separability may be analyzed with a hyper-plane, linearly non-separable data is analyzed with *kernel functions* such as higher order polynomials, Gaussian, and tan-sigmoid. The output of a SVM is a linear combination of the training examples projected on to a high dimensional feature space through the use of kernel functions. The Gaussian kernel gave the highest classification accuracy among the kernels tested. The value of the standard deviation was chosen as 0.2.

The NN, k-NN and mk-NN classifiers were implemented in C. For MLP and RBF, we have used Netlab, a package developed by C.M. Bishop and I.T. Nabney, Neural Computing Research group, Aston University, U.K. For SVM, we used SVM_ TORCH, a software developed by a group at IDIAP, Switzerland [16].

## VI. Results

Figure 1 shows the lung and liver areas in the fetal images, and the ROI's for extraction of textural features. Figure 2 gives the descriptive statistical details of the lung to liver feature values in the form of boxplots. It also characterizes the variation of the above features with respect to gestation age. Figure 3 demonstrates the dynamics of the selected features as a function of the gestation age for the lung and the liver. Figures 3A & 3B show that the fractal dimension and lacunarity of lung increase as a function of the gestation age. This is to be expected because the granularity of the cells change with the GA. Explicitly, the cells of the lung are found elongated during early gestation period, which could give rise to images that are quite smooth, that is, less granular in nature. However, the cells become spherical and fluid-filled [1] towards the term. Further, since the fluid to tissue content ratio changes with GA, the diffuse scattering properties also change, leading to more granular images.

Figure 3C shows a decrease in the echogenicity of lung as compared to the liver as GA increases. The echogenicity of the lung is almost the same as that of the liver at early GA. Thus, the lung seems to attenuate ultrasound waves more than the liver at later GA's (see [4]). The variance of the gray values of the lung (Fig. 3D) has an upward trend with GA, whereas that of the liver remains relatively unchanged throughout the period. The plot of CV (Fig. 3E) shows a similar trend as that of the variance and the plot of the second moment (Fig. 3F) is similar to that of FD. It may be noted that the nature of variation of the features of the liver is, in most cases, similar to that of the lung. Table 1 shows the results of classification. In all the cases we have less number of false negatives, which is a preferred outcome. The results indicate the consistency of classification.

## VII. Discussion

In the area of fetal monitoring, a reliable method to determine lung maturity is very essential. The use of ultrasound to study fetal lung maturity is advantageous over others because of its non-invasive nature. Traditionally, ultrasound has been used in fetal monitoring to obtain physical measurements of fetal size and placenta condition. In our work, pulmonary risk assessment based on ultrasound textural features has given encouraging results.

In our study, we have considered three different training and test sets as explained in the earlier section. This formulation is to test the generalization and adaptability of the classifiers. The first training set is more biased towards the immature class. We need our classifiers to be more sensitive and specific for immature class, because classification of immature class as mature is less desirable. If a mature lung is classified as immature, the problem is not very serious because adequate medical support would have been made available. The classifiers' accuracy for the training and test sets is given in Table 1. It may be noted that all the classifiers have almost comparable accuracy of classification, with NN and mk-NN having a little edge over the others. The number of false negatives is low for every classifier. The results show a high degree of specificity of the classifiers to the immature class.

In the second case, the training set did not contain any sample from 32 - 34 weeks, and the test set did not contain any sample from gestation ages below 32 weeks. This step was undertaken to ensure that the classifier is not biased by data, which could belong to either of the classes. Maturity does not occur before 32 weeks for a normal fetus, whereas it is guaranteed beyond 36 weeks [17]. Thus, the testing of images from the intervening period is likely to throw light on the transition period. An increase in the number of false negatives is seen in this case (see Table 1). This is because, we have assumed that the data corresponds to the immature class, whereas in reality, some of them could actually have transited to the mature class. As seen from the results, the NN classifier and its variants have performed poorly when compared to other classifiers, showing their poor generalization capability. In the third set, we had equal number of samples from both classes in order to have an unbiased training of the classifiers. From Table 1, we see that even in the case of unbiased training, the classification results are very consistent, with few false negatives. In fact, the results are very close to the biased training, and in the case of RBF and SVM classifiers, better than the latter.

The NN and mk-NN have given more accuracy where complete data set i.e samples from 24 to 38 weeks were used. When tested with samples only from 24 to 30 weeks (immature) and 36 to 38 weeks (mature), all the classifiers had comparable accuracy of classification. At the boundary between the two classes, the neighbourhood classifiers performed better. Their accuracy can be attributed to more closeness in the neighbourhood relation among the samples at the boundary of the two classes. The boundary samples along with the other samples of the two classes contribute for the greater accuracy of NN and mk-NN classifiers. The classification accuracy for $k$-NN and $mk$-NN was computed for various values of $k$ starting from $k$=2. The classification accuracy for the test sets decreased with increasing $k$ upto $k = 6$, increased for $k = 7 and 8$, and decreased once again for $k > 8$. Based on this test, the value of $k = 7$ was selected.

Some of the earlier studies have established usefulness of ultrasound examinations in predicting pulmonary maturity with various degrees of accuracy, by using features like, placenta grading, physical measurements of fetal size, echogenicites of the lung and liver regions, attenuation of frequencies in the lung and liver regions, and shift in the RF frequency spectrum during the process of maturation [2], [3], [5], [4], [6], [8]. In our study, we have used textural features as a measure of pulmonary maturation which has yielded an accuracy of classification from 73% to 96%. To the best of the authors' knowledge, this seems to be the first ever attempt to classify fetal lung maturity in terms of textural features of the ultrasound image. Since in all the cases, the lung and the liver have been imaged together, the effects due to the imaging techniques (including the internal processing by the machine) must affect both the regions similarly, and thus must not cause any variations on the textural features of the lung and liver differentially.

## VIII. Conclusion

In this study, it has been shown that the textural features are better indicators of the histological changes, compared to the study of only the echogenicity. Based on the results, it is clear that the fetal pulmonary risk can be fairly accurately assessed by studying the ultrasound images. This result is worth investigating further, because of its clinical ramifications. A complete sonographic analysis, which combines the above textural features with parameters such as fetal biparietal diameter, placental grading, femur length, head circumference and the abdominal circumference could possibly enhance the prediction accuracy. Also, an analysis of data from high risk pregnancies (mothers with hypertension or diabetes mellitus) could be used to further validate the prediction of maturity using sonographic features. Further investigation of textural features of ultrasound along with biochemical tests will help establish the validity of the method and eliminate the use of invasive tests for fetal pulmonary risk assessment.

## Acknowledgment

The authors convey their heartfelt thanks to Dr. S. Suresh, Consultant, Fetal Care Research Foundation, Chennai and Dr. Teresa W P Chow, Department of Obstetrics and Gynaecology, University of Malaya, Kuala Lumpur for their magnanimous help in providing the data and spending their valuable time in giving suggestions at different stages of the work and validating the results.

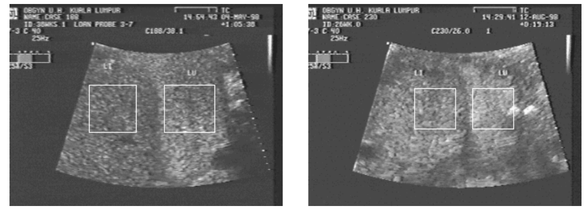

Fig. 1. Samples of fetal echogram with lung and liver regions and the regions of interest shown.

## References


[1] Thieme, M. Johnson, H. Silvers, Banjavic, and Carson, "Sonographic identification of lung maturation in fetal lamb," *Invest. Radiology*, vol. 18, pp. 18–26, 1983.

[2] W. J. Garrett, P. S. Warren, and R. H. Picker, "Maturation of the fetal lung, liver and bowel," *Radiology*, vol. 155, pp. 473–475, 1985.

[3] P. D. Cayea, D. C. Grant, P. M. Doubilet, and T. B. Jones, "Prediction of fetal lung maturity: inaccuracy of study using conventional ultrasound instruments," *Radiology*, vol. 155, pp. 473–475, 1985.

[4] D. M. Benson and L. D. Waldroup, "Ultrasonic tissue characterization of fetal lung, liver and placenta for the purpose of assessing fetal maturity," *J. Ultrasound in Medicine*, vol. 2, pp. 489–494, 1983.

[5] M. Feingold, J. Scollins, C. Cetrulo, and D. Koza, "Fetal lung to liver reflectivity ratio and lung maturity," *J. Clin. Ultrasound*, vol. 15, pp. 384–387, 1987.

[6] M. Podobnik, B. Brayer, and B. Ciglar, "Ultrasonic fetal and placenta tissue characterization and lung maturity," *Int. Jour. of Gynecology and Obstetrics*, vol. 54, pp. 221–229, 1996.

[7] R. A. Petrucha, S. H. Golde, and L. D. Platt, "The use of ultrasound in the prediction of fetal pulmonary maturity," *Am. J. Obestetrics and Gynecology*, vol. 144, no. 8, pp. 931–934, 1982.

[8] C. Sohn, W. Stolz, A. S. Gast, and G. Bastert, "Ultrasound diagnosis of fetal lung maturity," *Zentralbl Gynakol*, vol. 117, no. 3, pp. 138–143, 1995.

[9] U. Raeth, D. Schlaps, B. Limberg, I. Zuna, A. Lorenz, G. van Kaick, W. J. Lorenz, and B. Kommerell, "Diagnostic accuracy of computerised B-scan texture analysis and conventional ultasonography in diffuse parenchymal and malignant liver disease," *J. Clin. Ultras.*, vol. 13, pp. 87 –99, 1985.

[10] H. Huisman and J. Thijssen, "Adaptive texture feature extraction with application to ultrasonic image analysis," *Ultrasonic Img.*, vol. 20, pp. 132–148, 1998.

[11] R. M. Haralick, "Statistical and structural approaches to texture," *Proc. IEEE*, vol. 67(5), pp. 304–322, 1979.

[12] K. I. Laws, "Texture energy measures," in *Proc. Img. understanding Workshop*, vol. 0, pp. 47–51, 1979.

[13] J. M. Keller, S. Chen, and Crownover, "Texture description and segmentation through fractal geometry," *Computer Vision, Graphics and Image Processing*, vol. 45, pp. 150–166, 1989.

[14] S. Haykin, *Neural Networks : A Comprehensive Foundation.* Chap.4,5 and 6, Prentice Hall, 1999.

[15] V. Vapnik, *The Nature of Statistical Learning Theory.* New York: Springer, 1995.

[16] R. Collobert and S. Bengio, "On the convergence of SVMTorch, an algorithm for large scale regression problems," tech. rep., Dalle Molle Inst. for Perceptual Artificial Intelligence, Martigny, Switzerland, 2000.

[17] L. Gluck and M. V. Kulovich, "Fetal lung development: current concepts," *Pediatr. Clin. North Am.*, vol. 20, pp. 275–292, 1973.

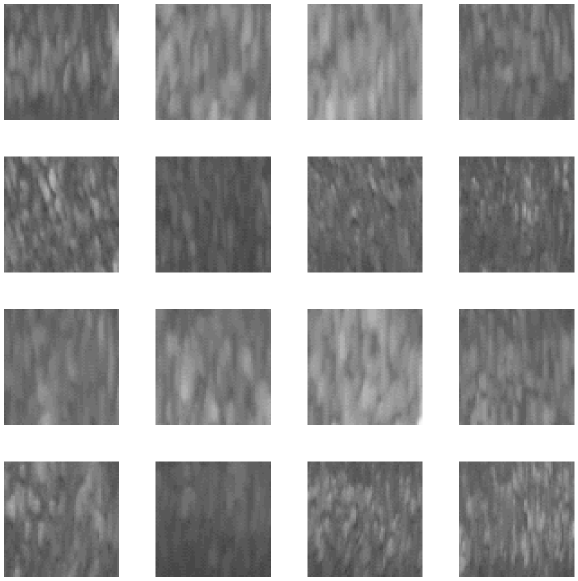

Fig. 2. Regions of interest from sample lung and liver images from GA 24 - 38 weeks. First two rows : Lung; Last two rows : Liver

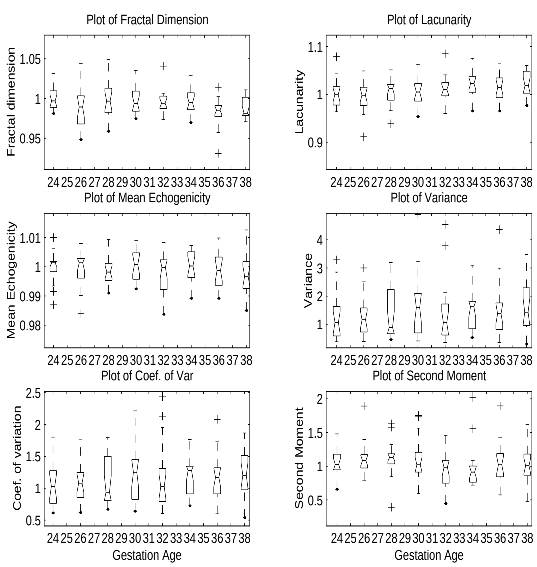


Fig. 3. Plots of ratios of lung-liver feature values as a function of gestation age

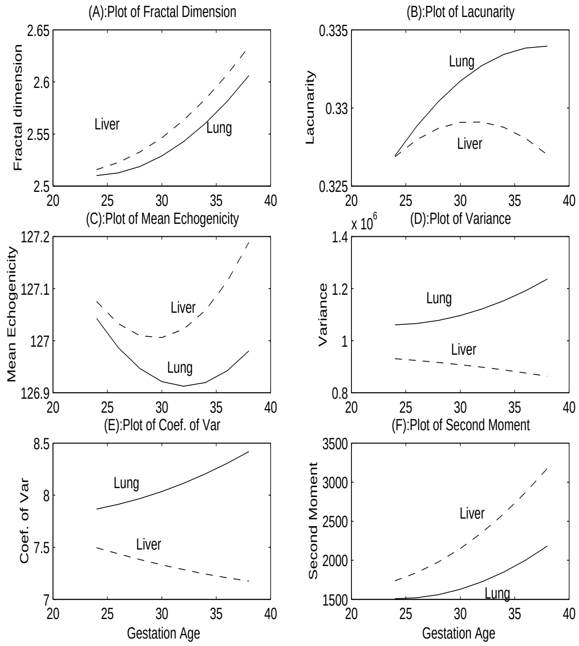


Fig. 4. Plots of texture features of lung and liver as a function of gestation age

TABLE I

Confusion matrix for various classifiers for test sets 1, 2 & 3 (I,M: immature and mature classes, CA: classification accuracy for test set FN: No. of false negatives)

| *Classifiers* | *Correct Class* | *Classifier output* | | | | | |
|---|---|---|---|---|---|---|---|
| | | Test set-1 | | Test set-2 | | Test set-3 | |
| | | I | M | I | M | I | M |
| | | 150 | 50 | 200 | 50 | 50 | 50 |
| **NN** | I | 145 | 5 | 170 | 30 | 46 | 4 |
| | M | 3 | 47 | 33 | 17 | 0 | 50 |
| | CA | 96% | | 74.8% | | 96% | |
| | FN | 5 | | 30 | | 4 | |
| **k- NN** | I | 142 | 8 | 164 | 36 | 44 | 6 |
| | M | 30 | 20 | 30 | 20 | 16 | 34 |
| | CA | 81% | | 73.6% | | 78% | |
| | FN | 8 | | 36 | | 6 | |
| **mk- NN** | I | 147 | 3 | 170 | 30 | 46 | 4 |
| | M | 15 | 35 | 14 | 36 | 5 | 45 |
| | CA | 91% | | 82.4% | | 91% | |
| | FN | 3 | | 30 | | 4 | |
| **MLP** | I | 150 | 0 | 187 | 13 | 46 | 4 |
| | M | 37 | 13 | 37 | 13 | 16 | 34 |
| | CA | 81.5% | | 80% | | 80% | |
| | FN | 0 | | 13 | | 4 | |
| **RBF** | I | 142 | 8 | 190 | 10 | 47 | 3 |
| | M | 30 | 20 | 43 | 7 | 14 | 36 |
| | CA | 81% | | 78.8% | | 83% | |
| | FN | 8 | | 10 | | 3 | |
| **SVM** | I | 142 | 8 | 165 | 35 | 47 | 3 |
| | M | 23 | 27 | 22 | 28 | 10 | 40 |
| | CA | 84.5% | | 77.2% | | 87% | |
| | FN | 8 | | 35 | | 3 | |